JCTC Journal of Chemical Theory and Computation

pubs.acs.org/JCTC Letter

Limits on the Precision of Catenane Molecular Motors: Insights from Thermodynamics and Molecular Dynamics Simulations

Alex Albaugh,[†] Rueih-Sheng Fu,[†] Geyao Gu, and Todd R. Gingrich*

Cite This: *J. Chem. Theory Comput.* 2024, 20, 1−6 Read Online

ACCESS | Metrics & More | Article Recommendations | Supporting Information

ABSTRACT: Thermodynamic uncertainty relations (TURs) relate precision to the dissipation rate, yet the inequalities can be far from saturation. Indeed, in catenane molecular motor simulations, we record precision far below the TUR limit. We further show that this inefficiency can be anticipated by four physical parameters: the thermodynamic driving force, fuel decomposition rate, coupling between fuel decomposition and motor motion, and rate of undriven motor motion. The physical insights might assist in designing molecular motors in the future.

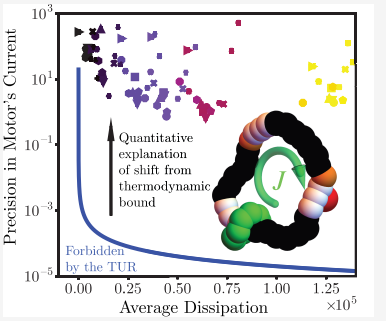

Molecular motors generate directed motion, extracting free energy from their environment and producing entropy in the process.[1] Biological motors like myosin,[2] dynein,[3] and ATP synthase[4] are responsible for important processes like muscle contraction, molecular transport, and chemical fuel generation, respectively. Recent breakthroughs in synthetic chemistry have also led to autonomous artificial motors that are chemically fueled.[5−11] With net flows of energy, molecular motor systems are necessarily out of equilibrium. Systems driven only weakly out of equilibrium can be analyzed with linear response theory, but molecular motors do not necessarily operate in such a regime. Limited tools are available for studying systems far from equilibrium, and the recent development of fluctuation theorems[12−14] and associated results have allowed for novel thermodynamic analyses of these systems.[15−17]

A family of such results, known collectively as thermodynamic uncertainty relations (TURs), governs the relationship between fluctuations in a time-extensive current J and the total dissipation Σ. TURs were first studied, postulated, and derived in the context of Markov jump processes in the long-time limit[18−20] and have since been generalized[21] to a wide variety of domains, such as Markov chains,[22] diffusions,[23−27] and quantum systems.[28−30] The classical overdamped TUR can be expressed in the form

$$\frac{\mathrm{var}(J)}{\langle J\rangle^2} \geq \frac{2k_B}{\langle \Sigma\rangle} \tag{1}$$

where k_B is the Boltzmann constant, $\langle\cdot\rangle$ is the mean, and $\mathrm{var}(\cdot)$ is the variance. A common biochemical situation is that the dissipation comes from the net decomposition of N_{rxn} fuel molecules, each feeling a thermodynamic driving force $\Delta\mu$ at temperature T. In that no-load case, the dissipation associated with the net reactions $\Sigma_{rxn} = N_{rxn}\Delta\mu/T$ can be viewed as a particular current of interest, allowing eq 1 to be translated into a restriction on the stochastic fluctuations in the number of fuel decomposition events:

$$\mathrm{var}(N_{rxn}) \geq \frac{2}{\beta\Delta\mu}\langle N_{rxn}\rangle \tag{2}$$

where $\beta = 1/k_BT$. TURs set a fundamental limit on the precision of fluctuating systems, so it is natural to characterize a motor's efficiency by how closely it saturates the corresponding TUR.[31] This measure of efficiency is meaningful even when a motor spins with no load. In that case, the thermodynamic efficiency, measured as work out per energy input, necessarily vanishes simply because there is no work with no load. By contrast, the efficiency we discuss measures how effectively the motor generates directed motion, something that can occur even in the absence of the load. Much of the literature surrounding TURs deals with relatively low-dimensional models and systems. Here, we demonstrate how a high-dimensional particle-based model of an artificial molecular motor can be used in conjunction with molecular dynamics simulations to generate a direct comparison against the TUR and explain how it can be employed in studying molecular motors. This effort complements current research

Received: October 30, 2023
Accepted: December 15, 2023
Published: December 21, 2023

https://doi.org/10.1021/acs.jctc.3c01201
J. Chem. Theory Comput. 2024, 20, 1−6

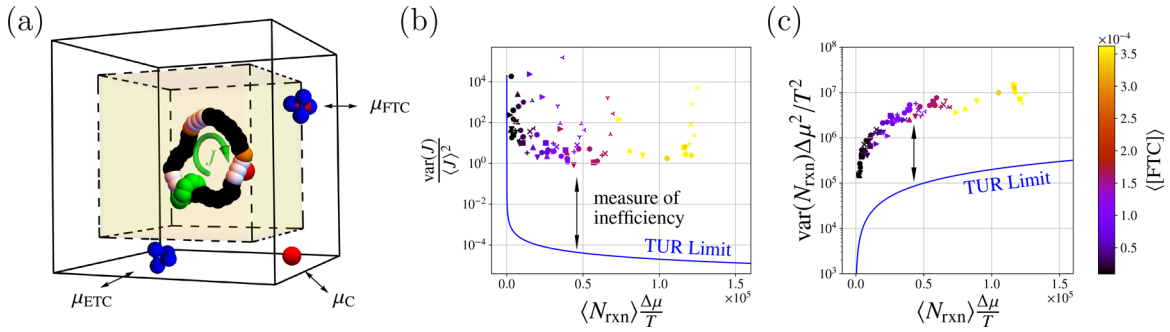

Figure 1. (*a*) The simulated motor model consisting of a green shuttling ring that diffuses around a larger ring and preferentially binds at orange sites. The net decomposition of N_{rxn} full tetrahedral clusters (FTC, red and blue) into empty tetrahedral clusters (ETC, blue) and free particles (C, red) couples to the motion of the shuttling ring and induces a time-integrated current J, which measures the net number of cycles in the clockwise direction. The coupling between the current and fuel decomposition results from attractive energetic interactions between the FTC clusters and the white binding sites, which catalyze fuel decomposition. By tuning the chemical potentials of the three species, μ_{FTC}, μ_{ETC}, and μ_C, we impose a nonequilibrium driving force $\Delta\mu = \mu_{FTC} - \mu_{ETC} - \mu_C$ via a grand canonical Monte Carlo procedure that tends to inject FTC into and remove ETC and C from the system at temperature T.[36] Plotted in (*b*) and (*c*) are comparisons of the data with the TUR limits eqs 1 and 2, respectively) for a family of catenane motors with varying numbers of binding and catalytic sites, friction, and backbone rigidity, denoted with different symbols (see Supporting Information (SI) Sec. I for details). We choose to express the x axis of each plot in terms of the typical dissipation $\langle\Sigma\rangle = \langle\Sigma_{rxn}\rangle = \langle N_{rxn}\rangle\Delta\mu/T$. The color bar denotes the concentration of FTC molecules, which is controlled by the associated chemical potential.

on the optimal control of and performance trade-offs for molecular motors.[32−35]

How efficiently a motor approaches the TUR limit is a complicated function of a high-dimensional design space. Depending on the interaction strengths between components of the motor, the motor can range from a precise machine to a dud, scenarios that we illustrate with molecular simulations of a family of catenane motors. Our main results offer quantitative measures of the degree of saturation of the TUR bound in these catenane motors. While the large design space yields motors with precisions varying over several orders of magnitude, we can anticipate how close each motor will get to the TUR bound by knowing just four physical properties: the chemical potential driving the motor, the rate of fuel decomposition, the coupling between fuel decomposition and motor motion, and the rate of undriven motor motion. We derive such a simplification using a minimal Markov model and illustrate that the resulting expressions, eqs 7 and 10, are instructive in explaining the performance of the more complicated molecular dynamics simulations of catenane motors. We further translate eq 10 into a biophysical context to explain why biological motors can operate orders of magnitude closer to the TUR bound than presently demonstrated artificial ones. Understanding how closely artificial molecular motors can saturate these fundamental TUR bounds highlights inefficiencies in their design and provides insight into how we might improve future artificial motors.

MOLECULAR MOTOR SIMULATIONS

We use a classical particle-based model of a molecular motor[36] inspired by the first synthetic, autonomous, chemically fueled molecular motor.[5] As shown in Figure 1a, the catenane motor consists of two interlocked rings. The smaller shuttling ring traverses the larger ring by diffusion. Both rings are composed of particles that are held together by nearest-neighbor bonds. The larger ring contains a number of motifs, each consisting of a binding site (shown in orange) directly adjacent to a catalytic site (shown in white). Binding sites act as potential energy wells for the shuttling ring, whereas catalytic sites facilitate the decomposition of fuel molecules present in the bulk.

The fuel is represented by a full tetrahedral cluster (FTC) that consists of two components: an empty tetrahedral cluster (ETC) and a central particle (C), which is kinetically trapped within the ETC. Whereas the motor is confined to an inner volume of the simulation box, the FTC, ETC, and C are free to pass between both inner and outer volumes. The fuel decomposes when the C escapes from the FTC to form the ETC and C. After a fuel decomposition event, the C may remain on the catalytic site for some time, resulting in steric hindrance that blocks the motion of the shuttling ring. Further, the presence of the shuttling ring at a binding site inhibits catalysis at the proximal catalytic site, again by steric hindrance. The resulting kinetic asymmetry couples the ring-and-fuel system and creates an information ratchet that gates the natural diffusion of the shuttling ring in a preferred direction.[36−39] Modifying the spacing between motifs on the large ring can even allow for control over the shuttling ring's preferred direction.[39]

The whole system undergoes Langevin dynamics interspersed with periodic grand canonical Monte Carlo (GCMC) moves in the outer volume that set up a nonequilibrium chemical potential gradient. The chemical potentials of the FTC, ETC, and C in the outer volume, μ_{FTC}, μ_{ETC}, and μ_C respectively, are fixed via GCMC moves,[36,40,41] which act as chemostats. By setting μ_{FTC} high and μ_{ETC} and μ_C low, we induce favorable conditions for fuel decomposition and generate a chemical potential gradient

$$\Delta\mu = \mu_{FTC} - \mu_{ETC} - \mu_C \tag{3}$$

that tends to introduce the FTC into the system and simultaneously remove the ETC and C from it. This simulation setup allows us to perform numerical experiments with varying motor configurations, pair potentials, chemical potentials, frictions, and temperatures. Results from the array of simulations are all plotted together in Figure 1 with the color of the plot markers reflecting the fuel concentration and the symbols representing motors with different characteristics, as described further in the SI.

https://doi.org/10.1021/acs.jctc.3c01201
J. Chem. Theory Comput. 2024, 20, 1−6

DISSIPATION

Each step in the simulation is microscopically reversible so that the dissipation can be rigorously computed as the entropy production in the reservoirs. Due to local detailed balance with those reservoirs, the entropy produced during a single trajectory $\mathbf{x}$ studied for an observation time t_{obs} can equivalently be measured by the statistical irreversibility of the trajectory. From that perspective, the entropy production associated with the trajectory, $\Sigma(\mathbf{x})$, is expressed as the log-ratio of the probability of observing $\mathbf{x}$ to its time-reversed analogue $\tilde{\mathbf{x}}$,[42]

$$\Sigma(\mathbf{x}) = k_B \ln \frac{P(\mathbf{x})}{P(\tilde{\mathbf{x}})} \tag{4}$$

An individual trajectory is stochastic because of random thermal noise from the Langevin dynamics and the addition and removal of the FTC, ETC, and C via GCMC moves. These factors combine multiplicatively to form $P(\mathbf{x})$ and $P(\tilde{\mathbf{x}})$, allowing Σ to be computed directly from simulations via eq 4. That total entropy production can be decomposed into components arising from the Langevin dynamics[43,44] and the chemostats. The decomposition, shown explicitly in the SI, illustrates that the average entropy production can equivalently be computed from the entropy production of the reaction alone: $\langle\Sigma\rangle = \langle\Sigma_{rxn}\rangle = \langle N_{rxn}\rangle\Delta\mu/T$.

THE CURRENT AND ITS PRECISION

To analyze the TURs, we must compare this typical entropy production to the fluctuations of time-integrated currents. Two such currents are N_{rxn} and the physical current that counts the net displacement of the shuttling ring around the large ring in its preferred direction, a current we call J. Means and variances of both currents are readily extracted by sampling simulated trajectories. In the case of N_{rxn} this merely requires that one count how many net FTC decompositions have occurred in a given time t_{obs}. For J, one counts the net number of large-ring particles that the shuttling ring passes Δn in that same t_{obs}.

Figures 1b and 1c show the precision of the currents for a variety of model configurations and operating conditions and how they compare to the TURs for J and N_{rxn}, eqs 1 and 2, respectively. Both currents and their precisions depend strongly on μ_{FTC}. In alignment with the governing TURs, increasing the FTC concentration generally drives more current and decreases its relative variance. However, for both J and N_{rxn}, the magnitude of the precision is far from the TUR bound—5 orders of magnitude for J and 2 for N_{rxn}—implying stark inefficiency that we subsequently rationalize. Interestingly, the precision of N_{rxn} appears to collapse onto a single curve in Figure 1c, suggesting that the data are governed by some TUR-like relationship between the mean and variance.

A MINIMAL MODEL OF A LOOSELY COUPLED MOTOR

To pursue the idea that appropriately rescaled data would collapse onto a TUR-like relationship, we introduce a minimal Markov model for which we could analytically compute such a rescaling. This minimal model should share the essential structure of the simulated catenane motors. For example, the simulations reveal a loosely coupled motor; only some of the fuel decompositions actually result in the directed motion of the shuttling ring. The loose coupling motivates us to introduce a minimal Markov model that involves three distinct events: fuel-coupled ring motion, fuel-decoupled ring motion, and futile fuel reactions. In terms of this simple model, we are able to quantitatively reproduce the features discussed in Figure 1, which allows us to identify the factors that contribute to the looseness of the bounds. The model also enables straightforward analyses of design strategies for altering the motor to tighten these bounds.

The Markov model, illustrated in Figure 2, consists of a shuttling ring that hops along an infinite track with binding

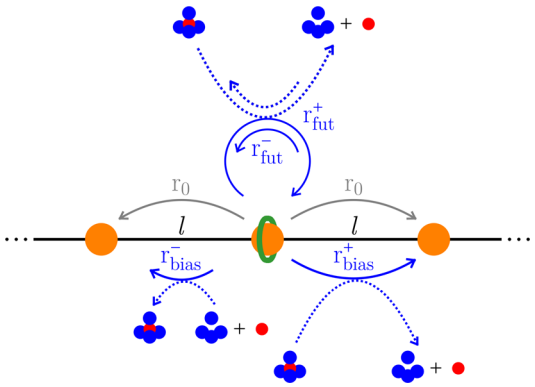

Figure 2. Schematic of a minimal model of a loosely coupled motor. Each state in the model represents a binding site on the large ring separated by a distance l. Movement between these states corresponds to the shuttling ring hopping between binding sites. There are three different types of dynamic events that can occur: biased motion with rates $r^{\pm}_{bias}$, unbiased motion with rate r_0, and futile fuel decomposition with rates $r^{\pm}_{fut}$. As illustrated, certain events are coupled to the decomposition or reconstitution of fuel, and others are not. Explicit expressions for the rates of each event are provided in the main text.

sites separated by a distance l. This infinite track can be thought of as the result of unfurling the large ring of the catenane into a linear track with periodic replicas. We focus on the coupling between the motion of the shuttling ring and the fuel transformation events, whereby fuel transformation refers both to the decomposition of the FTC to form the waste products ETC and C and to the reconstitution of the FTC from the ETC and C. At each moment in time, one of three dynamical events can take place: fuel transformation coupled to biased motion with rates $r^{\pm}_{bias}$, futile fuel transformation not coupled to motion with rates $r^{\pm}_{fut}$, and unbiased motion not coupled to fuel transformation with rate r_0. The superscript + denotes decomposition of fuel, whereas the superscript − denotes reconstitution of fuel. Fuel transformation is coupled to biased motion in the sense that the decomposition of one unit of fuel causes the ring to move one hop in the favored direction, cf. Figure 2. Therefore, the ring dynamics are modeled as a superposition of a symmetric random walker perfectly decoupled from fuel dynamics and an asymmetric random walk perfectly coupled to fuel dynamics. The degree of coupling is quantified as the proportion of the fuel transformation coupled to biased motion.

The rates of the Markov model can be recast in terms of parameters with clear physical meaning: ζ, the combined rate of unbiased movement events; λ, the combined rate of fuel transformation events; η, the proportion of fuel transformation coupled to biased motion; and $\Delta\mu$, the change in free energy associated with the decomposition of a single FTC species in solution, as calculated for the particle simulations in the SI.[45] For thermodynamic consistency, each forward move must have

https://doi.org/10.1021/acs.jctc.3c01201
J. Chem. Theory Comput. 2024, 20, 1−6

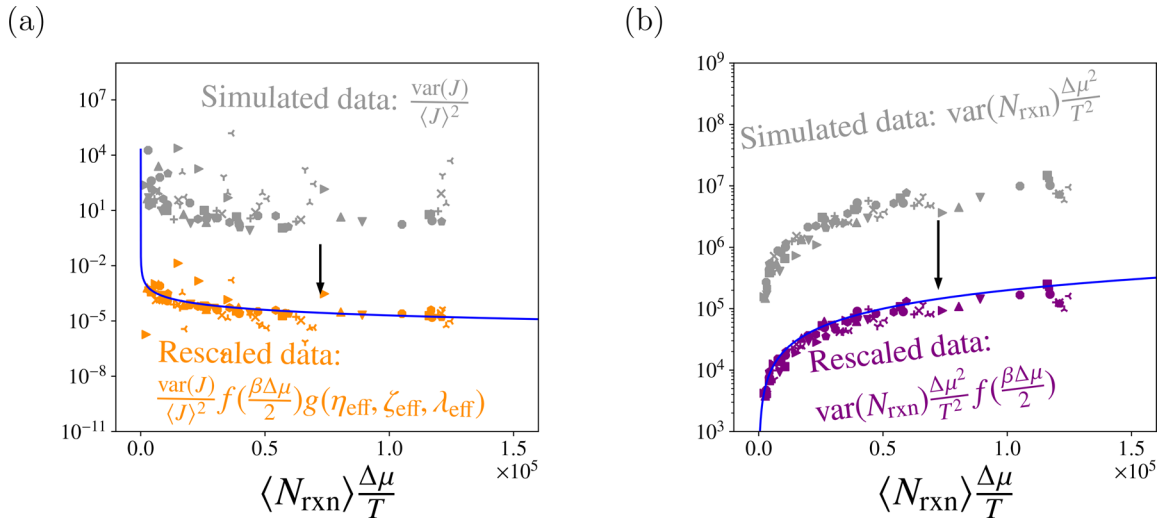

Figure 3. Plots showing the rescaling of eqs 11 and 12 applied to the simulated J and N_{rxn} current fluctuations from molecular dynamics simulations of catenane motors. That the rescaled fluctuations lie on the curves of the TUR bounds indicates that the analytical scaling factors quantify how far the fluctuations are from the TUR bounds.

a reverse counterpart. The ratio of rates for these pairs of moves is proportional to the exponential of the free energetic difference that drives the bias. Because the ring has degenerate binding sites, microscopic reversibility requires $r^+ = r^- \exp(\beta\Delta\mu)$. Furthermore, by definition, the rate of biased motion must be $\eta\lambda$, and that for futile fuel transformation must be $(1-\eta)\lambda$. These constraints uniquely specify the rates $r^+_{\mathrm{bias}} = r^-_{\mathrm{bias}} e^{\beta\Delta\mu} = \eta\lambda/(1+e^{-\beta\Delta\mu})$, $r^+_{\mathrm{fut}} = r^-_{\mathrm{fut}} e^{\beta\Delta\mu} = (1-\eta)\lambda/(1+e^{-\beta\Delta\mu})$, and $r_0 = \zeta/2$. The particle simulation operates under conditions in which $\beta\Delta\mu \gg 1$ and hence $r^+ \gg r^-$.

CURRENT FLUCTUATIONS IN THE MINIMAL MODEL

We let N^+_0, N^-_0, N^+_{fut}, N^-_{fut}, N^+_{bias}, and N^-_{bias} be the number of forward (+) and reverse (−) moves accrued in time t_{obs} due, respectively, to unbiased motion, futile fuel decomposition, and fuel decomposition coupled to biased motion. With the Markovian assumption, these variables are all Poisson distributed, with parameters equal to the corresponding rates multiplied by t_{obs}. Both the shuttling-ring and fuel-decomposition currents can be expressed in terms of those Poisson variables: $J = (N^+_{\mathrm{bias}} - N^-_{\mathrm{bias}} + N^+_0 - N^-_0)l$ and $N_{\mathrm{rxn}} = N^+_{\mathrm{bias}} - N^-_{\mathrm{bias}} + N^+_{\mathrm{fut}} - N^-_{\mathrm{fut}}$, where l is the length scale separating the binding sites in Figure 2. Making use of the fact that a Poisson-distributed N with the parameter $r\cdot t_{\mathrm{obs}}$ has $\langle N\rangle = \mathrm{var}(N) = r\cdot t_{\mathrm{obs}}$, the mean and variance of J and N_{rxn} in the Markov model can be calculated. For N_{rxn}, that calculation yields

$$\langle N_{\mathrm{rxn}}\rangle = \lambda t_{\mathrm{obs}} \tanh\left(\frac{\beta\Delta\mu}{2}\right) \tag{5}$$

$$\mathrm{var}(N_{\mathrm{rxn}}) = \lambda t_{\mathrm{obs}} \tag{6}$$

which can be rearranged into

$$\mathrm{var}(N_{\mathrm{rxn}}) f\left(\frac{\beta\Delta\mu}{2}\right) = \frac{2}{\beta\Delta\mu}\langle N_{\mathrm{rxn}}\rangle \tag{7}$$

an *equality* resembling the TUR *inequality*, eq 2. Here, the saturation of the TUR inequality is determined by the scaling factor $f(x) = \tanh(x)/x$, which tends to 1 as $\beta\Delta\mu$ vanishes. For the Markov model of Figure 2, we see that the tightness of the N_{rxn} fluctuations relative to its TUR bound is exclusively regulated by $\beta\Delta\mu$, the dimensionless free energy of decomposition.

Repeating the Poisson analysis for J gives the mean and variance

$$\langle J\rangle = \eta\lambda \tanh\left(\frac{\beta\Delta\mu}{2}\right) t_{\mathrm{obs}} l \tag{8}$$

$$\mathrm{var}(J) = (\eta\lambda + \zeta) t_{\mathrm{obs}} l^2 \tag{9}$$

Rearrangement yields

$$\frac{\mathrm{var}(J)}{\langle J\rangle^2} f\left(\frac{\beta\Delta\mu}{2}\right) g(\eta, \zeta, \lambda) = \frac{2k_{\mathrm{B}}}{\langle\Sigma\rangle} \tag{10}$$

an *equality* resembling the current TUR *inequality*, eq 1. Now, the saturation of the TUR for J is determined by $f(\beta\Delta\mu/2)$ and $g(\eta,\zeta,\lambda) = \eta^2\lambda/(\eta\lambda + \zeta)$. The same factor $f(\beta\Delta\mu/2)$ that appeared in eq 7 reflects that the minimal model's saturation of the TUR for fuel decomposition is necessary but insufficient to also saturate the TUR for J.

The TUR equalities, eqs 7 and 10, only rigorously apply to the minimal Markov model. It is not obvious that they would provide direct insight into the fluctuations in the more complicated simulations. The minimal Markov model imagines independently varying ζ, η, λ, and $\Delta\mu$, but modifying motor interactions in the molecular dynamics simulations simultaneously changes all four parameters. Remarkably, we show that for a broad array of motor designs, both eqs 7 and 10 are able to describe the simulation fluctuations if the Markov model parameters ζ, η, and λ are replaced by effective values ζ_{eff}, η_{eff}, and λ_{eff} extracted from the simulations, as described in the SI.

To the extent that the minimal Markov model captures the simulated fluctuations, eqs 7 and 10 therefore imply that the TUR inequalities would be converted into equalities if we rescaled variances:

$$\mathrm{var}(J) \to \mathrm{var}(J) f\left(\frac{\beta\Delta\mu}{2}\right) g(\eta_{\mathrm{eff}}, \zeta_{\mathrm{eff}}, \lambda_{\mathrm{eff}}) \tag{11}$$

https://doi.org/10.1021/acs.jctc.3c01201
J. Chem. Theory Comput. 2024, 20, 1−6

$$\mathrm{var}(N_{\mathrm{rxn}}) \rightarrow \mathrm{var}(N_{\mathrm{rxn}}) f\left(\frac{\beta\Delta\mu}{2}\right) \tag{12}$$

Figure 3 shows the result of applying that rescaling on the simulation data. The rescaled fluctuations are effectively mapped onto the TUR curves, implying that the rescaling factors f and g are measures of how close the fluctuations get to saturating the TUR inequalities. Crucially, because these f and g factors are expressed in terms of physically interpretable parameters, it allows us to address how those physical quantities (the chemical potential driving the motor, the rate of fuel decomposition, the coupling between fuel decomposition and motor motion, and the rate of undriven motor motion) impact the degree of TUR saturation.

DISCUSSION

The TUR has attracted great interest because the inequality connecting motor precision with thermodynamics is generic, but the generality of the result can obscure the fact that far-from-equilibrium machines can operate far from the TUR bound. Indeed, in our simulations of an artificial catenane motor, we have shown that the fluctuations in current deviate from the TUR bound by 5−6 orders of magnitude. Even when the TUR is loose, we have here demonstrated that we can closely approximate the fluctuations in terms of the TUR via the rescaling of eqs 11 and 12. This connection allows us to attribute the observed deviations from the TUR to both the large free energy difference driving fuel decomposition ($\beta\Delta\mu$ ranged from 74 to 118 for our numerical experiments) and the low current from lack of coupling between fuel decomposition and ring movement (η_{eff} ranged from 0 to 0.11). Both $\Delta\mu$ and coupling are clearly important factors in considering motor performance,[46,47] and $f(\beta\Delta\mu/2)$ and $g(\eta_{\mathrm{eff}}, \eta_{\mathrm{eff}}, \lambda_{\mathrm{eff}})$ now quantitatively highlight their impact on current fluctuations in these catenane motors.

From the rescaling, we see that minimizing the deviation from the TUR requires a combination of tight coupling and low entropy production from fuel decomposition. TUR saturation simultaneously demands perfect coupling ($\eta_{\mathrm{eff}} = 1$), a vanishing driving force ($\Delta\mu \rightarrow 0$), and no unbiased movement ($\zeta = 0$). It is suggestive to compare with biophysical motors driven by ATP hydrolysis, which for physiological conditions means $\Delta\mu \approx 20k_{\mathrm{B}}T$ and $f(\beta\Delta\mu/2) \approx 0.1$. That $\Delta\mu$ places a limit on the maximal achievable precision, but unlike our catenane simulations, the g term will have a limited role in most biophysical situations. The difference is that the biophysical motors typically benefit from tight mechanical coupling[48] between fuel decomposition and mechanical motion, so that $\eta \approx 1$, $\zeta \ll 1$, and $g(\eta_{\mathrm{eff}}, \zeta_{\mathrm{eff}}, \lambda_{\mathrm{eff}}) \approx 1$. Without realizing similar tight coupling in synthetic motors, it will be hard to engineer them to reach the precision of their biophysical counterparts.

ASSOCIATED CONTENT

Supporting Information

The Supporting Information is available free of charge at https://pubs.acs.org/doi/10.1021/acs.jctc.3c01201.

Simulation details, model of the motor, derivation of entropy production terms, calculations for the minimal model, free energy and entropy of the decomposition reaction, bulk contributions to the TUR bound, simulated motor precision and produced entropy compared to the general TUR, and motor precision compare to the current TUR (PDF)

AUTHOR INFORMATION

Corresponding Author

Todd R. Gingrich − *Department of Chemistry, Northwestern University, Evanston, Illinois 60208, United States;* orcid.org/0000-0003-4617-7146; Email: todd.gingrich@northwestern.edu

Authors

Alex Albaugh − *Department of Chemical Engineering and Materials Science, Wayne State University, Detroit, Michigan 48202, United States;* orcid.org/0000-0002-3091-0369

Rueih-Sheng Fu − *Department of Chemistry, Northwestern University, Evanston, Illinois 60208, United States;* orcid.org/0000-0003-0181-2636

Geyao Gu − *Department of Chemistry, Northwestern University, Evanston, Illinois 60208, United States;* orcid.org/0000-0002-4266-4716

Complete contact information is available at: https://pubs.acs.org/10.1021/acs.jctc.3c01201

Author Contributions

†A.A. and R.-S.F. contributed equally to this work.

Notes

The authors declare no competing financial interest.

ACKNOWLEDGMENTS

We gratefully acknowledge insightful discussions with Emanuele Penocchio. Research reported in this publication was supported by the Gordon and Betty Moore Foundation through Grant No. GBMF10790.

REFERENCES

(1) Brown, A. I.; Sivak, D. A. Theory of nonequilibrium free energy transduction by molecular machines. *Chem. Rev.* **2020**, *120*, 434−459.

(2) Finer, J. T.; Simmons, R. M.; Spudich, J. A. Single myosin molecule mechanics: Piconewton forces and nanometre steps. *Nature* **1994**, *368*, 113−119.

(3) Schnapp, B. J.; Reese, T. S. Dynein is the motor for retrograde axonal transport of organelles. *Proc. Natl. Acad. Sci. U. S. A.* **1989**, *86*, 1548−1552.

(4) Yasuda, R.; Noji, H.; Kinosita, K., Jr; Yoshida, M. F1-ATPase is a highly efficient molecular motor that rotates with discrete 120 steps. *Cell* **1998**, *93*, 1117−1124.

(5) Wilson, M. R.; Solà, J.; Carlone, A.; Goldup, S. M.; Lebrasseur, N.; Leigh, D. A. An autonomous chemically fuelled small-molecule motor. *Nature* **2016**, *534*, 235−240.

(6) Borsley, S.; Leigh, D. A.; Roberts, B. M. W. A doubly kinetically-gated information ratchet autonomously driven by carbodiimide hydration. *J. Am. Chem. Soc.* **2021**, *143*, 4414−4420.

(7) Borsley, S.; Kreidt, E.; Leigh, D. A.; Roberts, B. M. W. Autonomous fuelled directional rotation about a covalent single bond. *Nature* **2022**, *604*, 80−85.

(8) Korosec, C. S.; Jindal, L.; Schneider, M.; de la Barca, I. C.; Zuckermann, M. J.; Forde, N. R.; Emberly, E. Substrate stiffness tunes the dynamics of polyvalent rolling motors. *Soft Matter* **2021**, *17*, 1468−1479.

(9) Erbas-Cakmak, S.; Leigh, D. A.; McTernan, C. T.; Nussbaumer, A. L. Artificial molecular machines. *Chem. Rev.* **2015**, *115*, 10081−10206.

(10) Unksov, I. N.; Korosec, C. S.; Surendiran, P.; Verardo, D.; Lyttleton, R.; Forde, N. R.; Linke, H. Through the Eyes of Creators:

Observing Artificial Molecular Motors. *ACS Nanoscience Au* **2022**, *2*, 140−159.
(11) Amano, S.; Fielden, S. D. P.; Leigh, D. A. A catalysis-driven artificial molecular pump. *Nature* **2021**, *594*, 529−534.
(12) Evans, D. J.; Searles, D. J. The fluctuation theorem. *Adv. Phys.* **2002**, *51*, 1529−1585.
(13) Rao, R.; Esposito, M. Detailed fluctuation theorems: A unifying perspective. *Entropy* **2018**, *20*, 635.
(14) Esposito, M.; Van den Broeck, C. Three detailed fluctuation theorems. *Phys. Rev. Lett.* **2010**, *104*, No. 090601.
(15) Seifert, U. Fluctuation theorem for a single enzym or molecular motor. *Europhys. Lett.* **2005**, *70*, 36.
(16) Andrieux, D.; Gaspard, P. Fluctuation theorems and the nonequilibrium thermodynamics of molecular motors. *Phys. Rev. E* **2006**, *74*, No. 011906.
(17) Pietzonka, P.; Zimmermann, E.; Seifert, U. Fine-structured large deviations and the fluctuation theorem: Molecular motors and beyond. *Europhys. Lett.* **2014**, *107*, No. 20002.
(18) Barato, A. C.; Seifert, U. Thermodynamic uncertainty relation for biomolecular processes. *Phys. Rev. Lett.* **2015**, *114*, No. 158101.
(19) Gingrich, T. R.; Horowitz, J. M.; Perunov, N.; England, J. L. Dissipation bounds all steady-state current fluctuations. *Phys. Rev. Lett.* **2016**, *116*, No. 120601.
(20) Pietzonka, P.; Barato, A. C.; Seifert, U. Universal bounds on current fluctuations. *Phys. Rev. E* **2016**, *93*, No. 052145.
(21) Falasco, G.; Esposito, M.; Delvenne, J.-C. Unifying thermodynamic uncertainty relations. *New J. Phys.* **2020**, *22*, No. 053046.
(22) Proesmans, K.; Van den Broeck, C. Discrete-time thermodynamic uncertainty relation. *EPL (Europhysics Letters)* **2017**, *119*, No. 20001.
(23) Polettini, M.; Lazarescu, A.; Esposito, M. Tightening the uncertainty principle for stochastic currents. *Phys. Rev. E* **2016**, *94*, No. 052104.
(24) Gingrich, T. R.; Rotskoff, G. M.; Horowitz, J. M. Inferring dissipation from current fluctuations. *Journal of Physics A: Mathematical and Theoretical* **2017**, *50*, No. 184004.
(25) Van Vu, T.; Hasegawa, Y. Uncertainty relations for underdamped Langevin dynamics. *Phys. Rev. E* **2019**, *100*, No. 032130.
(26) Lee, J. S.; Park, J.-M.; Park, H. Universal form of thermodynamic uncertainty relation for Langevin dynamics. *Phys. Rev. E* **2021**, *104*, No. L052102.
(27) Fischer, L. P.; Pietzonka, P.; Seifert, U. Large deviation function for a driven underdamped particle in a periodic potential. *Phys. Rev. E* **2018**, *97*, No. 022143.
(28) Carollo, F.; Jack, R. L.; Garrahan, J. P. Unraveling the large deviation statistics of Markovian open quantum systems. *Phys. Rev. Lett.* **2019**, *122*, No. 130605.
(29) Guarnieri, G.; Landi, G. T.; Clark, S. R.; Goold, J. Thermodynamics of precision in quantum nonequilibrium steady states. *Physical Review Research* **2019**, *1*, No. 033021.
(30) Hasegawa, Y. Thermodynamic uncertainty relation for general open quantum systems. *Phys. Rev. Lett.* **2021**, *126*, No. 010602.
(31) Song, Y.; Hyeon, C. Thermodynamic uncertainty relation to assess biological processes. *J. Chem. Phys.* **2021**, *154*, No. 130901.
(32) Pietzonka, P.; Barato, A. C.; Seifert, U. Universal bound on the efficiency of molecular motors. *Journal of Statistical Mechanics: Theory and Experiment* **2016**, *2016*, No. 124004.
(33) Leighton, M. P.; Sivak, D. A. Performance scaling and trade-offs for collective motor-driven transport. *New J. Phys.* **2022**, *24*, No. 013009.
(34) Gupta, D.; Large, S. J.; Toyabe, S.; Sivak, D. A. Optimal Control of the F1-ATPase Molecular Motor. *J. Phys. Chem. Lett.* **2022**, *13*, 11844−11849.
(35) Lathouwers, E.; Lucero, J. N. E.; Sivak, D. A. Nonequilibrium energy transduction in stochastic strongly coupled rotary motors. *J. Phys. Chem. Lett.* **2020**, *11*, 5273−5278.
(36) Albaugh, A.; Gingrich, T. R. Simulating a chemically fueled molecular motor with nonequilibrium molecular dynamics. *Nat. Commun.* **2022**, *13*, 2204.
(37) Astumian, R. D. Running on information. *Nat. Nanotechnol.* **2016**, *11*, 582−583.
(38) Amano, S.; Esposito, M.; Kreidt, E.; Leigh, D. A.; Penocchio, E.; Roberts, B. M. W. Insights from an information thermodynamics analysis of a synthetic molecular motor. *Nat. Chem.* **2022**, *14*, 530.
(39) Albaugh, A.; Gu, G.; Gingrich, T. R. Sterically driven current reversal in a molecular motor model. *Proc. Natl. Acad. Sci. U. S. A.* **2023**, *120*, No. e2210500120.
(40) Frenkel, D.; Smit, B. *Understanding Molecular Simulation: From Algorithms to Applications*; Elsevier, 2001; Vol. *1*.
(41) Chempath, S.; Clark, L. A.; Snurr, R. Q. Two general methods for grand canonical ensemble simulation of molecules with internal flexibility. *J. Chem. Phys.* **2003**, *118*, 7635−7643.
(42) Seifert, U. Entropy production along a stochastic trajectory and an integral fluctuation theorem. *Phys. Rev. Lett.* **2005**, *95*, No. 040602.
(43) Sivak, D. A.; Chodera, J. D.; Crooks, G. E. Using nonequilibrium fluctuation theorems to understand and correct errors in equilibrium and nonequilibrium simulations of discrete Langevin dynamics. *Physical Review X* **2013**, *3*, No. 011007.
(44) Sivak, D. A.; Chodera, J. D.; Crooks, G. E. Time step rescaling recovers continuous-time dynamical properties for discrete-time Langevin integration of nonequilibrium systems. *J. Phys. Chem. B* **2014**, *118*, 6466−6474.
(45) Shirts, M. R.; Chodera, J. D. Statistically optimal analysis of samples from multiple equilibrium states. *J. Chem. Phys.* **2008**, *129*, No. 124105.
(46) Borsley, S.; Leigh, D. A.; Roberts, B. M. W.; Vitorica-Yrezabal, I. J. Tuning the force, speed, and efficiency of an autonomous chemically fueled information ratchet. *J. Am. Chem. Soc.* **2022**, *144*, 17241−17248.
(47) Borsley, S.; Leigh, D. A.; Roberts, B. M. W. Chemical fuels for molecular machinery. *Nat. Chem.* **2022**, *14*, 728−738.
(48) Soga, N.; Kimura, K.; Kinosita, K., Jr; Yoshida, M.; Suzuki, T. Perfect chemomechanical coupling of FoF1-ATP synthase. *Proc. Natl. Acad. Sci. U. S. A.* **2017**, *114*, 4960−4965.

https://doi.org/10.1021/acs.jctc.3c01201
J. Chem. Theory Comput. 2024, 20, 1−6